Digital Signal Processing 131 (2022) 103759

Contents lists available at ScienceDirect

Digital Signal Processing

www.elsevier.com/locate/dsp

A GNSS meta-signal SAGE-based multipath-mitigating loop design

Ning Chang [a,b,*], Xi Hong [a], Wenjie Wang [a], Gonzalo Seco-Granados [b]

[a] Ministry of Education Key Lab for Intelligent Networks and Network Security, Xi'an Jiaotong University, Xi'an, 710049, China
[b] Department of Telecommunications and Systems Engineering, CERES-IEEC, Universitat Autònoma de Barcelona, Barcelona, 08193, Spain

ARTICLE INFO

Article history:
Available online 3 October 2022

Keywords:
GNSS multi-antenna receiver
Meta-signal
SAGE
Multipath mitigation
Loop design

ABSTRACT

A major challenge suffered by Global Navigation Satellite System (GNSS) receivers is the multipath interference, which results in serious tracking performance degradation and increased positioning errors. Growing evidence suggests that wide-bandwidth signals and multi-antenna technology are set to become two vital factors to improve the GNSS multipath mitigation, leading to the concept of meta-GNSS signal and multi-dimensional processing. To estimate the time delay of line-of-sight (LOS) ray in a multipath environment, we propose a meta-signal Space Alternating Generalized Expectation (SAGE) based locked loop (SAGELL) design, which exploits the high-resolution of the meta-signal together with the characteristics from spatial and temporal domains. The SAGELL design comprises two main setups: the SAGE-based discriminator and combinational loops. Benefiting from the multi-dimensional processing and meta-signal bandwidth, the SAGE-based discriminator first estimates the LOS ray and the multipath rays in single side-band components and achieves the global estimates of the dual side-band components coherently. Aiming to accurately track each ray of the meta-signal, we further close the SAGELL via angle, code phase, and carrier phase locked loops to filter and predict the estimates. The proposed GNSS meta-signal multipath-mitigating loop design allows for GNSS high-precision discrimination and tracking in multipath scenarios, even in the presence of highly correlated rays, as confirmed by the numerical results.

1. Introduction

Positioning information is usually provided by modern Global Navigation Satellite Systems (GNSS), such as GPS, Galileo, and Beidou. A major challenge imposed on GNSS receivers is the multipath interference produced by signal reflections coming from various objects [1], resulting in severe tracking performance degradation and positioning error increase [2], [3]. Such positioning inaccuracy is particularly detrimental for applications with submeter accuracy requirements, like car collision avoidance and lane-level navigation, as the multipath error induced in the pseudoranges can reach meters or even hundreds of meters in traditional GNSS receivers [4], [5]. Therefore, how to efficiently tackle multipath mitigation continues to be one of the critical aspects in GNSS.

Numerous representative multipath mitigation methods for standard GNSS signals have been developed in the past decades. With respect to single-antenna GNSS receiver, the narrow Early-Late Discriminator (nEML) [6] and Multipath Estimating Delay Locked Loop (MEDLL) [7], [8] are some of the most popular methods. The former reduces the spacing between the early and late correlators. While the latter is a time Maximum Likelihood (ML) estimator together with parallel interference cancellation to combat multipath. However, nEML and MEDLL unfortunately come with limited multipath discrimination capabilities, as only the signal feature from temporal domain is exploited. Thanks to a significant leap forward in multi-antenna technology, the spatial domain provides additional degrees of freedom resolving multipath. Building upon the multi-antenna GNSS receiver, several efforts that jointly exploits the spatial, temporal, and frequential features have been devoted to multipath parameter estimation. In [9–11], the subspace-based approaches decompose the vectorized GNSS signal, achieving a favorable balance between multipath discriminating ability and complexity. Considering the sparse spatial and temporal characteristics, the compressed sensing-based approaches [12], [13] stand out in multipath mitigation with low carrier-to-noise ratios (C/N_0) and few snapshots. Nevertheless, neither the subspace-based nor the compressed sensing-based approaches achieve optimal performance owing to the rank-deficient covariance matrix [14] in multipath environment and the off-grid effect [15], respectively. In contrast with the two kinds of aforementioned approaches, the Space Alternating Generalized Expectation Maximization algorithm (SAGE), a sequential approximation of the

* Corresponding author at: Ministry of Education Key Lab for Intelligent Networks and Network Security, Xi'an Jiaotong University, Xi'an, 710049, China.
E-mail addresses: changning@stu.xjtu.edu.cn (N. Chang), harryhong@stu.xjtu.edu.cn (X. Hong), wjwang@mail.xjtu.edu.cn (W. Wang), Gonzalo.Seco@uab.cat (G. Seco-Granados).

https://doi.org/10.1016/j.dsp.2022.103759
1051-2004/

ML-based estimator [16], [17], can attain a higher accuracy that is close to Cramér-Rao lower bound (CRLB) and with improvements regarding the trade-off between convergence rate and complexity [18]. In addition to the successful application of parameter estimation in mobile radio environment, it has been shown that SAGE is also a promising candidate to combat multipath for GNSS due to its multi-dimensional processing with fast convergence and low complexity [18–20].

The insights gained from the multi-dimensional processing can be of assistance in strengthening multipath mitigation. However, most of these works have considered the narrowband GNSS signal case. The narrow-bandwidth, in general, can only cope with the multipath discrimination under a large time delay difference between the line-of-sight (LOS) ray and the multipath rays and is therefore restricted to the meter-level ranging accuracy. To handle the multipath mitigation of GNSS system that has highly correlated rays, a direct but efficient solution is to break the bandwidth limitation of narrowband signal (The large-bandwidth signal allows the narrower main peak of auto-correlation function (ACF), hence a better temporal resolution). Therefore, meta-GNSS signal, a paradigm of multi-signal combination based on two different GNSS signals transmitted at different carrier frequencies [21], [22] has recently received significant interest in academia. It is expected that the typical meta-signal reaches bandwidths of tens or hundreds of megahertz and hence can fundamentally support a superior tracking accuracy and promising multipath mitigation [23].

Several approaches and estimators are available to perform time delay estimation for meta-signals, categorized into direct meta-signal processing and double side-band (DSB) processing. The former involves considering the meta-signal as a whole using a meta-signal local replica at the receiver, thus following the matched filter principle [24]. The researchers in [25–27] directly adopt an ML-based solution to the whole meta-signal and analyze the corresponding CRLBs. Since the spectra of the constituent side-band signals may result in a large bandwidth, the sampling rate can even reach hundreds of megahertz, which seriously aggravates the complexity burden [28]. In order to reduce the complexity, the matched filter can be equivalently implemented by splitting it into two different matched filters in DSB processing, one corresponding to each side-band signal, which are then coherently combined. This approach was adopted, for instance, in the pioneering work [22] via two ML-based estimators, laying a solid foundation for DSB processing of the meta-signal. Later on, the classical double estimator technique was proposed for Binary Offset Carrier (BOC) signals in [29], with extensions to combat the multipath in [30], [31]. Due to the similar frequency separation characteristic to meta-signal, this method was ingeniously applied to meta-signal processing in [32–34]. As a consequence of the double loops for code and subcarrier, ambiguities are diminished to some extent. Although the existing meta-signal processing methods are shown to have the decimeter-or centimeter-level ranging accuracy, all these discussions were carried out under the ideal precondition of single ray. While for the meta-signal paradigm in a more practical multipath condition, several relevant investigations, including the detailed working mechanism and the fundamental capability in terms of multipath mitigation, have not been explored yet.

In this paper, in order to maintain a high accuracy of LOS time delay estimation in multipath environment, we exploit the synergy between the robustness of multi-dimensional processing and the excellent characteristic of the meta-signal. A multi-dimensional GNSS meta-signal loop design, the SAGE-based lock loop (SAGELL), is proposed to combat multipath, leveraging the merits of both the SAGE algorithm and wide-bandwidth. Specifically, this paper makes the following contributions.

- The analyses of typical GNSS meta-signals, including the descriptions of power spectrum densities (PSDs) and auto-correlation functions (ACFs), the multipath-induced ACFs, and spatial-temporal meta-signal spectra, are provided. The analyses above demonstrate the necessity and feasibility of differentiating multipath by multi-dimensional processing and meta-signal.
- Considering the goal of both high accuracy and low complexity, we establish a multipath-mitigating SAGE-based discriminator for SAGELL design through a divide-and-conquer principle. First, the individual side-band components of the meta-signal are characterized by joint spatial, temporal, and frequential domains, then the LOS ray and the multipath rays are resolved via parallel cancellation. Next, we coherently combine the estimates of individual signals into some global estimates to achieve the high multipath-mitigating performance profiting from wide bandwidth of the meta-signal. Finally, the first two steps iterate until the SAGE-based discriminator converges.
- To better filter and predict each ray of the meta-signal, three kinds of loops: angle locked loops (ALL), delay locked loops (DLL), and carrier phase locked loops (PLL), are jointly set to track both LOS ray and multipath rays. The application of these loops helps the SAGELL precisely form the predicted results to initialize the SAGE-based discriminator in the next period.
- We compare the SAGELL design in two aspects: the maximum error envelopes (MEEs) and the root mean square errors (RMSEs) via C/N_0 with the state-of-art methods. As the MEE simulations show, the SAGELL possesses an outstanding multipath-mitigating capability that could not be achieved by processing the signal in spatial and temporal domains alone. Additionally, the RMSEs of SAGELL reaches the theoretical performance bound in one ray condition and surpasses the comparisons in multipath conditions (especially in severe multipath condition). All the simulation results indicate the SAGELL a promising multipath-mitigating loop design.

The remainder of this paper is structured as follows. Section 2 introduces the system model of the meta-signal. The character analysis of the meta-signal is presented in Section 3. In Section 4, we present the principle of SAGE and the SAGELL design. Simulation results will be demonstrated in Section 5. Finally, we conclude this paper in Section 6.

Notations: Matrices are denoted by capital letters in boldface (e.g., $\boldsymbol{A}$), and vectors are denoted by lowercase letters in boldface (e.g., $\boldsymbol{a}$). $(\cdot)^T$, $(\cdot)^H$, denote the matrix transpose and the Hermitian transpose, respectively.

2. Meta-signal model

Consider a meta-signal $\boldsymbol{y}(t)$ composed of left side-band component $\boldsymbol{y}^L(t)$ and right side-band component $\boldsymbol{y}^R(t)$ whose spectra are placed side-by-side with respect to a central frequency by frequency offsets $-f_s$ and f_s, respectively. We assume the wavefield of the meta-signal is generated by one LOS ray and K multipath rays arriving from angles $\boldsymbol{\theta}$ with corresponding time delays $\boldsymbol{\tau}$, the Doppler frequency offsets (DFO) $\boldsymbol{f}_d$, and the carrier phase offsets $\boldsymbol{\phi}$, where $\boldsymbol{\theta} \doteq [\theta_0, \ldots, \theta_K]^T$, $\boldsymbol{\tau} \doteq [\tau_0, \ldots, \tau_K]^T$, $\boldsymbol{f}_d \doteq \left[f_{d,0}, \ldots, f_{d,K}\right]^T$, and $\boldsymbol{\phi} \doteq [\phi_0, \ldots, \phi_K]^T$. According to the previous considerations, the complex-equivalent baseband signal $\boldsymbol{y}(t)$ received at the output of an M element array can be expressed as

$$\boldsymbol{y}(t) = \boldsymbol{y}^L(t) + \boldsymbol{y}^R(t)$$

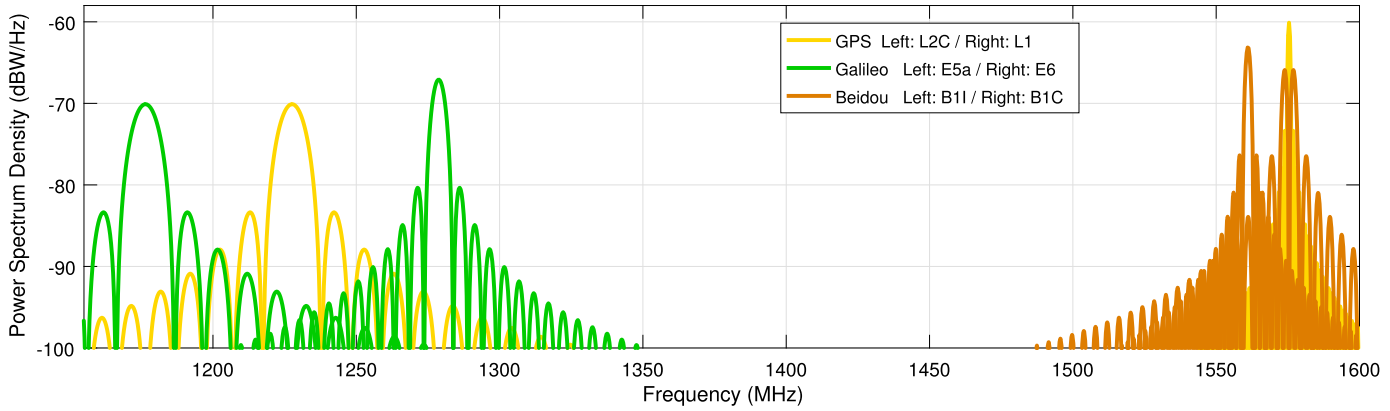

Fig. 1. PSDs of typical meta-signals. (For interpretation of the colors in the figure(s), the reader is referred to the web version of this article.)

$$= \sum_{k=0}^{K} \boldsymbol{a}^L(\theta_k)\, \alpha_k^L c^L(t-\tau_k)\, e^{j(-2\pi f_s t + 2\pi f_s \tau_k)} e^{j(2\pi f_{d,k} t + \phi_k)} + \boldsymbol{n}^L(t)$$

$$+ \sum_{k=0}^{K} \boldsymbol{a}^R(\theta_k)\, \alpha_k^R c^R(t-\tau_k) e^{j(2\pi f_s t - 2\pi f_s \tau_k)} e^{j(2\pi f_{d,k} t + \phi_k)} + \boldsymbol{n}^R(t) \quad (1)$$

where the superscript L and R denote the affiliation with the left and right component, respectively. For the two side-band components, the steering vectors $\boldsymbol{a}^L(\theta_k)$ and $\boldsymbol{a}^R(\theta_k)$, amplitudes α_k^L and α_k^R, and code waveforms $c^L(t)$ and $c^R(t)$ τ_k are set for the kth ray. Notice that $c^L(t)$ and $c^L(t)$ can be directly code with a Binary Phase Shift Keying (BPSK) modulation, or a BOC type modulation [35]. The phase offsets $2\pi f_s \tau_k$ and $-2\pi f_s \tau_k$ of the kth ray are the subcarrier phase offsets introduced by time delay, which are vital in attaining high precision estimates. The carrier phase offset ϕ_k of the kth ray is defined as ϕ_k. The Gaussian noise contributions, uncorrelated with the signals, are represented as $\boldsymbol{n}^L(t)$ and $\boldsymbol{n}^R(t)$.

In this context, we assume that the number of rays K is already known, as several novel methods can be applied to determine K efficiently, e.g., classical criteria including [36], [37] and more advance techniques like [38], [39]. Moreover, the ionospheric effect [40], [41] across the wide reception band is assumed to be ignored or compensated for the following two reasons. In the case of modulated on very close frequencies, two side-band components from one satellite share the same reference clock and undergo nearly identical propagation paths to the receiver, resulting in strong coherence between these two components. As a result, the ionospheric effect across tens of megahertz can be ignored. Otherwise, in case the ionospheric transmission-induced time delays and carriers between two components are non-negligible, they can be estimated and compensated [42], but this is beyond the scope of this paper.

3. Characteristic analysis of meta-signal

This section first presents the characteristics of the representative meta-signals from the perspective of PSD and ACF. Then, the multipath-induced ACFs of the meta-signals are examined. A spatial-temporal spectrum of the meta-signal is also provided and discussed as an improved solution to multipath mitigation.

3.1. Brief introduction of meta-signal

Meta-signal is defined as an ensemble of two different frequency band GNSS signals, and hence has a wider bandwidth compared to standard GNSS signals. This wide-bandwidth property allows the meta-signal to obtain a better time-resolution, therefore more precise ranging accuracy. Any pair of synchronized signals could be in principle chosen, however the signals from the same satellite and modulated on adjacent frequencies are more appropriate than others [22] that they enjoy the same propagation path and similar time delay between the two components in meta-signal. Among a couple of discussed examples, this section will examine the three combinations in detail: the GPS L1 and L2C signals transmitted on L-band, the Galileo E5a and E6 signals transmitted on E-band, and the Beidou B1I and B1C signals transmitted on B-band. The characteristics of the meta-signal are given in terms of PSD and ACF, as follows.

The PSD of the meta-signal is approximated by the sum of the PSDs of the left and right side-band components [29]. As the bandwidth of the meta-signal is normally spaced by greater than several megahertz, the vast majority of the spectrum of each component of the meta-signal does not overlap, which allows for negligible interaction between the two components of the spectrum. The PSDs of typical meta-signals are shown in Fig. 1.

To display the potential of the meta-signal more intuitively, we next discuss the ACF of the meta-signal [22], which can be derived as follows,

$$\begin{aligned} R(\Delta\tau) &= R^L(\Delta\tau) + R^R(\Delta\tau) \\ &= R_{c^L}(\Delta\tau)\, e^{j2\pi f_s \Delta\tau} + R_{c^R}(\Delta\tau)\, e^{-j2\pi f_s \Delta\tau} \end{aligned} \quad (2)$$

where $R_{c^L}(\Delta\tau)$ and $R_{c^R}(\Delta\tau)$ denote the ACFs of the left and right side-band component, respectively. The corresponding ACFs of three typical meta-signals are depicted in Fig. 2.

In the two figures above, we show the PSDs of typical meta-signals and compare the main ACF peaks, where as expected, a wider PSD implies a narrower ACF and hence a higher time resolution. In particular, the ACF main peaks of typical meta-signals are evidently narrower compared to the ACF peaks of standard GNSS signals. The main peak of B-band meta-signal of Beidou B1I and B1C signals, for example, is just about one-fourteenth as large as that of GPS L1 of C/A signal. The above performance indicates that such a high-resolution meta-signal is a very powerful feature for multipath mitigation. A detailed description of the different GNSS meta-signals' main characteristics is given in Table 1.

3.2. Characteristic analysis of meta-signal in multipath case

The main peak of ACF has a sharp almost triangular shape, which facilitates multipath mitigation theoretically, as shown in Fig. 2. However, the ACF will be seriously deformed in practical multipath environments. To verify the multipath effect on the meta-signal, we consider two rays: one LOS ray with one multipath ray, and the time delay of the LOS ray is assumed as $0T_c$. The direct-signal-to-multipath-signal-amplitude ratio is assumed to be 6 dB and we take the Beidou B1I-B1C signals as the meta-signal

Table 1
Meta-signals main characteristics.

Signals		Modulation	Frequency (MHz)	Bandwidth (MHz)	ACF Main Peak
GPS	L2C L1	BPSK(10) BPSK(1)	1227.6 1575.42	347.82	$\pm 0.0029T_c$
Galileo	E5a E6	BPSK(10) BPSK(5)	1176.45 1278.75	102.3	$\pm 0.0098T_c$
Beidou	B1I B1C Data	BPSK(2) BOC(1,1)	1561.098 1575.42	14.322	$\pm 0.07T_c$

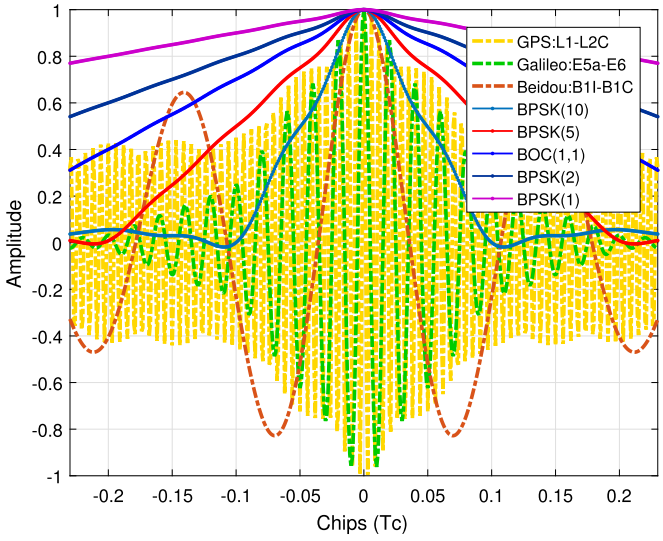

Fig. 2. ACFs of different satellite signals and meta-signals.

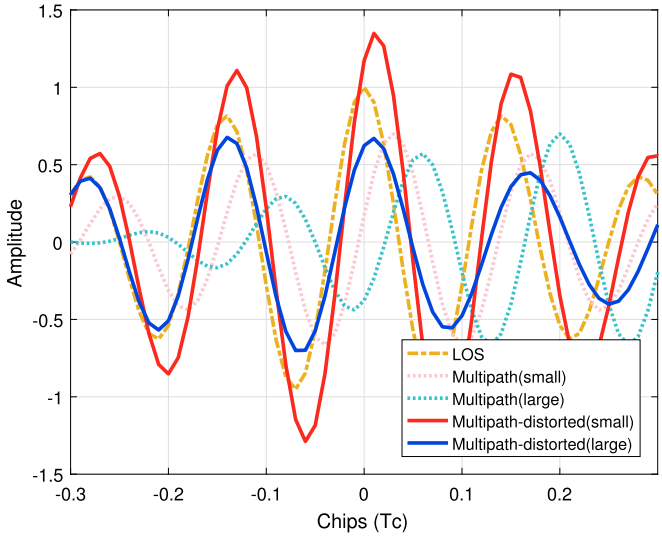

Fig. 3. ACFs of the meta-signals in multipath situation.

example. When the time delay difference between the LOS ray and the multipath ray is large, i.e., on the order of magnitude or larger than the width of the main peak (the time delay of the multipath ray is assumed to be $0.2T_c$), the amplitudes of the peaks change and a side peak can become higher than the central one, as depicted in the red curve of Fig. 3. When the time delay difference between the LOS ray and the multipath ray is small, i.e., restricted in the main peak (the time delay of the multipath ray here is assumed to be $0.03T_c$), then the shape of the main peak is distorted,

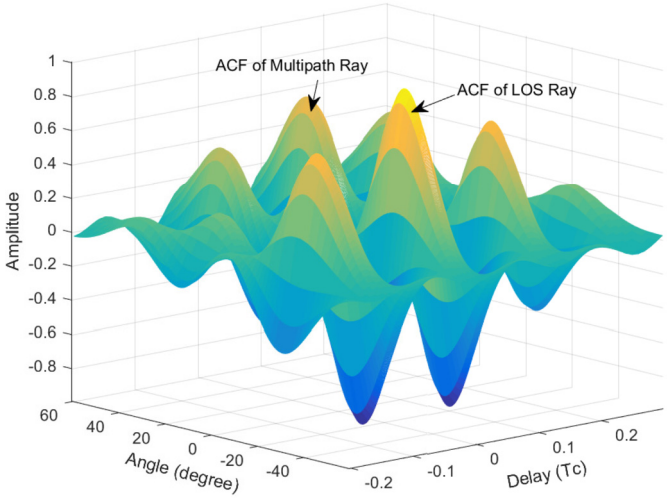

Fig. 4. Spatial-temporal spectrum of the meta-signal in multipath situation.

as demonstrated in the blue curve of Fig. 3. The ACFs in above two cases are distorted and they may highly probably lead to inaccurate estimation of LOS ray.

3.3. Spatial and temporal processing of meta-signal

To tackle the multipath mitigation, especially in the presence of highly temporally correlated signals, the multi-antenna technology can be efficiently exploited, as it provides extra spatial degrees of freedom. With the help of the spatial domain, we can observe the LOS and the multipath rays from multiple characteristics, such as angle and time delay. Fig. 4 illustrates the spatial and temporal spectrum of Beidou B-band meta-signal received by the multi-antenna array within the same settings in Fig. 3. Note that this spectrum is directly acquired by two-dimensional ML method in spatial and temporal domains.

The result in Fig. 4 shows that the LOS ray and the multipath ray are undoubtedly discriminated thanks to the joint use of spatial and temporal domains, and two perfect triangle-shaped ACFs are observed. Besides, the sharp main peak of each separated ACF indicates the excellent time delay estimation accuracy. Inspired by this spatial and temporal meta-signal spectrum, such a combination of multi-dimensional processing and meta-signal is expected to further improve the multipath mitigation.

4. SAGE-based locked loop design for meta-signal

Based on the above analyses, we next investigate the specific processing structure that is dedicated to meta-signal. In particular, several techniques are available: 1) The SAGE iteratively deals with multipath mitigation from multi-dimensions and provides precise descriptions for each ray. 2) The broadband advantage of the meta-signal contributes to high-accuracy estimates and to the improve-

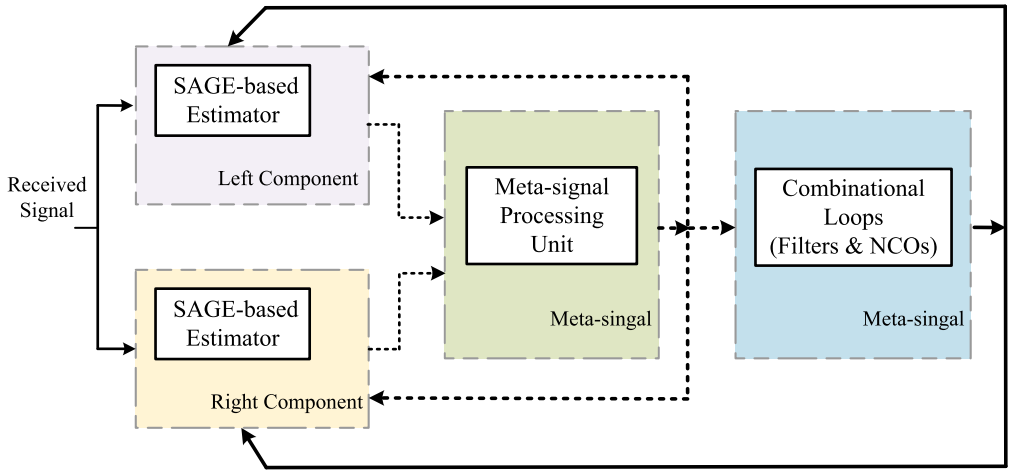

Fig. 5. SAGELL overview.

ment of multipath mitigation in temporal domain. 3) Numerous types of loops: ALLs, DLLs, and PLLs, can be extended to filter and predict each ray. How to incorporate the above techniques into a multipath-mitigating loop design achieving multipath mitigation (even in highly correlated rays) is our major concern. In the upcoming section, we first discuss the basic concept of the SAGE algorithm and then introduce the proposed SAGELL design from its structure to the whole scheme.

4.1. SAGE algorithm

The derivation of SAGE relies on the two key notions: the complete (unobservable) and incomplete (observable) data. In the problem of estimating superimposed single side-band meta-signals, referring to the equation (1), the individually observable signal[1] $\boldsymbol{s}_k^L(t)$ is expressed as

$$\begin{aligned}\boldsymbol{s}_k^L(t) &\doteq \boldsymbol{s}_k^L\left(t;\boldsymbol{\xi}_k^L,\alpha_k^L\right)\\ &= \alpha_k^L \boldsymbol{a}^L(\theta_k)\, c^L(t-\tau_k)\, e^{-j2\pi f_s(t-\tau_k)} e^{j(2\pi f_{d,k}t+\phi_k)}\end{aligned} \tag{3}$$

based on previous parameter estimate vector $\boldsymbol{\xi}_k \doteq \left[\theta_k, \tau_k, f_{d,k}, \phi_k\right]$ of the kth ray for the left side-band component. Corrupted by a part of the additive noise, the equation

$$\boldsymbol{x}_k^L(t) \doteq \boldsymbol{s}_k^L(t) + \boldsymbol{n}_k^L(t) \tag{4}$$

constitutes the natural set of complete data [19]. The received side-band component $\boldsymbol{y}_k^L(t)$ is identified with the incomplete data. It is related to the received signal according to $\boldsymbol{y}^L(t) = \sum_{k=0}^{K} \boldsymbol{x}_k^L(t)$.

Since $\boldsymbol{x}_k^L(t)$ is not observable, one can try to estimate it based on the observation $\boldsymbol{y}^L(t)$ of the incomplete data and previous estimates. A natural estimate of $\boldsymbol{x}_k^L(t)$ is its conditional expectation (Expectation-step) which is given by

$$\hat{\boldsymbol{x}}_k^L(t) = \boldsymbol{y}^L(t) - \sum_{k'=0, k'\neq k}^{K} \boldsymbol{s}_{k'}^L(t) \tag{5}$$

To get parameters estimated, including angles, time delays, DFOs, amplitudes and carrier phase offsets for each ray, the Maximization-step is presented,

$$\begin{aligned} &z\left(\theta_k, \tau_k, f_{d,k}\right)\\ &\quad\doteq \left(\boldsymbol{a}^L(\theta_k)\right)^H \hat{\boldsymbol{x}}_k^L(t) \left(c^L(t-\tau_k)\, e^{-j2\pi f_s(t-\tau_k)} e^{j2\pi f_{d,k}t}\right)^H \end{aligned} \tag{6a}$$

$$\hat{\theta}_k = \arg\max_{\theta} \left\{ \left| z\left(\theta_k, \hat{\tau}_k, \hat{f}_{d,k}\right)\right|^2 \right\} \tag{6b}$$

$$\hat{\tau}_k = \arg\max_{\tau} \left\{ \left| z\left(\hat{\theta}_k, \tau_k, \hat{f}_{d,k}\right)\right|^2 \right\} \tag{6c}$$

$$\hat{f}_{d,k} = \arg\max_{f_d} \left\{ \left| z\left(\hat{\theta}_k, \hat{\tau}_k, f_{d,k}\right)\right|^2 \right\} \tag{6d}$$

$$\hat{\alpha}_k = \left| z\left(\hat{\theta}_k, \hat{\tau}_k, \hat{f}_{d,k}\right)\right| \Big/ M_\theta \tag{6e}$$

$$\hat{\phi}_k = \text{angle}\left(z\left(\hat{\theta}_k, \hat{\tau}_k, \hat{f}_{d,k}\right)\right) \tag{6f}$$

where the multi-dimensional procedure is turned into single-dimensional ones. It should be noted that, although SAGE ensures the multipath mitigation while reducing the complexity, it tends to fall into local optimality due to its sensitivity against initialization in a multipath environment. Any initialization algorithms that provide practical spatial and temporal initial values can be arbitrarily selected, for examples [43], [20]. To initial the SAGELL, in this paper, we use a joint spatial and temporal sparse representation algorithm to estimate the coarse time delays and angles for all rays of the meta-signal via DSB processing. Please refer to the reference [13] for more details.

4.2. SAGELL for meta-signal

To attain a centimeter-level ranging accuracy in a multipath case, the multi-dimensional estimator SAGE and meta-signal are a good combination. Moreover, with the help of various ALLs, DLLs, and PLLs, the design of SAGELL for meta-signal can resolve and track each ray. As shown in Fig. 5, the SAGELL design for meta-signal is generally divided into two distinct sections: the SAGE-based discriminator (the purple, yellow, and green parts) and the combinational tracking loops (the blue part). The SAGE-based discriminator contributes to multipath mitigation by means of iterative SAGE and meta-signal. The two SAGE-based estimators are respectively based on left and right component of the meta-signal and the meta-signal processing unit is responsible for coherent or noncoherent combination of all the estimates. The whole procedure of discriminator tends to follow the dotted lines. To keep a low resource consumption, we take the divide-and-conquer processing into account that the SAGE-based discriminator consists of two SAGE-based estimators and one meta-signal processing unit.

[1] To avoid repetition, the left side-band component of the meta-signal is taken as an example. The SAGE algorithm of the right side-band component can be processed in a similar way.

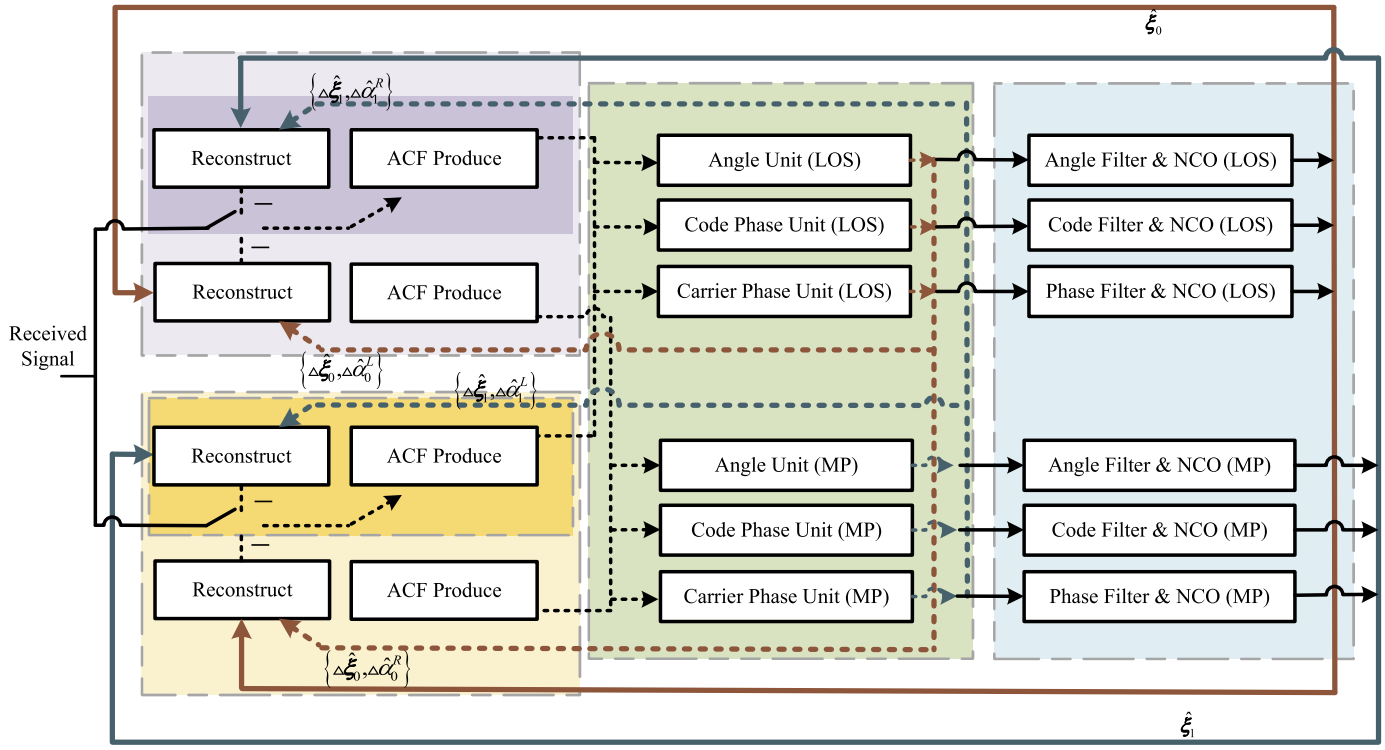

Fig. 6. SAGELL structure.

More specifically, we could expand the SAGELL to analyze the signal processing, as the specific description of SAGELL structure demonstrated in Fig. 6. (The parts of the same color in the two Figs. 5 and 6 have the same function.)

1). SAGE-based estimator for side-band component (the purple and yellow parts): We here carry out two SAGE-based estimators to sequentially separate each ray of left and right side-band component. The black dotted lines show the process in each side-band estimator. Firstly, the observable side-band signals $\left\{\boldsymbol{s}_k^L(t), \boldsymbol{s}_k^R(t)\right\}$ are reconstructed based on the updated variables $\left\{\Delta\hat{\alpha}_k^L, \Delta\hat{\alpha}_k^R, \Delta\hat{\boldsymbol{\xi}}_k\right\}$ obtained by the SAGE-based discriminator and the results $\hat{\boldsymbol{\xi}}_k$ predicted in the last loop period. Secondly, the unobservable side-band signals $\left\{\boldsymbol{x}_k^L(t), \boldsymbol{x}_k^R(t)\right\}$ are achieved through the Expectation-step. Thirdly, with the help of Maximization-step, we acquire the estimated spatial ACFs $\left\{\hat{R}_{\theta,k}^L\left(\Delta\theta_k^L\right), \hat{R}_{\theta,k}^R\left(\Delta\theta_k^R\right)\right\}$, the temporal ACFs $\left\{\hat{R}_{\tau,k}^L\left(\Delta\tau_k^L\right), \hat{R}_{\tau,k}^R\left(\Delta\tau_k^R\right)\right\}$, and the prompt correlators $\left\{\hat{P}_{\phi,k}^L\left(\Delta\phi_k^L\right), \hat{P}_{\phi,k}^R\left(\Delta\phi_k^R\right)\right\}$ for each side-band component.

2). Meta-signal processing (the green part): In order to obtain high accuracy of time delay estimation, we take advantage of the meta-signal characteristics, such as wide-bandwidth and strong coherence between the two components. The estimated ACFs and prompt correlators of each SAGE-based estimator are sent to the angle, code phase, and carrier phase units to coherently or incoherently form the global parameters, namely, angle $\Delta\hat{\theta}_k$, time delay $\Delta\hat{\tau}_k$, and carrier phase $\Delta\hat{\phi}_k$. These variables, along with the amplitudes $\left\{\Delta\hat{\alpha}_k^L, \Delta\hat{\alpha}_k^R\right\}$ for each ray are further updated through iterations going inside the whole SAGE-based discriminator. It is reminded that the process of entire meta-signal shall be observed through the colored dotted lines.

Regarding the tracking loops (the blue part) where the process flow goes after the solid lines, the parameters (angles, time delays, and carrier phases) for each ray merged by the meta-signal processing unit are sent into the corresponding ALLs, DLLs and PLLs for filtering and predicting. These functions can be realized by common filters and numerically-controlled oscillators (NCOs) in GNSS locked loops [44]. The precise prediction results $\hat{\boldsymbol{\xi}}_k$ are fed back to the next tracking period for initialization of SAGE-based discriminator.

4.2.1. SAGE-based estimator for side-band component

Now we take a more detailed look at the SAGE-based discriminator, including the purple, yellow and green parts, considering the particular case of the SAGE-based estimator that there is one LOS ray and one multipath ray of each side-band component. The further specification referring to the SAGE-based discriminator for meta-signal is displayed in Fig. 7.

Based on the prediction results in SAGELL, the estimated parameter vectors $\hat{\boldsymbol{\xi}}_0$ and $\hat{\boldsymbol{\xi}}_1$, and the estimated amplitudes $\left\{\Delta\hat{\alpha}_0^L, \Delta\hat{\alpha}_1^L, \Delta\hat{\alpha}_0^R, \Delta\hat{\alpha}_1^R\right\}$, the reconstructed multipath ray $\boldsymbol{s}_1^L(t)$ (referring to the reconstruct module in Fig. 6) can be expressed as

$$\begin{aligned}\boldsymbol{s}_1^L(t) &\doteq \boldsymbol{s}_1^L\left(t; \hat{\boldsymbol{\xi}}_1, \Delta\hat{\alpha}_1^L\right) \\ &= \Delta\hat{\alpha}_1^L \boldsymbol{a}^L\left(\hat{\theta}_1\right) c^L\left(t-\hat{\tau}_1\right) e^{-j2\pi f_s\left(t-\hat{\tau}_1\right)} e^{j\left(2\pi\hat{f}_{d,1}t+\hat{\phi}_1\right)}\end{aligned} \tag{7}$$

The residual part is defined as the estimated LOS ray $\hat{\boldsymbol{x}}_0^L(t)$, i.e., an unobservable one,

$$\hat{\boldsymbol{x}}_0^L(t) = \boldsymbol{y}^L(t) - \sum_{k'=0, k'\neq 0}^{K} \boldsymbol{s}_{k'}^L(t) \tag{8}$$

Thus, the variables for the LOS ray of left side-band component, such as the spatial ACF $\hat{R}_{\theta,0}^L\left(\Delta\theta_0^L\right)$, the temporal ACF $\hat{R}_{\tau,0}^L\left(\Delta\tau_0^L\right)$, the prompt correlator $\hat{P}_{\phi,0}^L\left(\Delta\phi_0^L\right)$, and its amplitude $\Delta\hat{\alpha}_0^L$ are estimated successively (referring to the ACF module in Fig. 6). They can be approximately denoted as the equations,

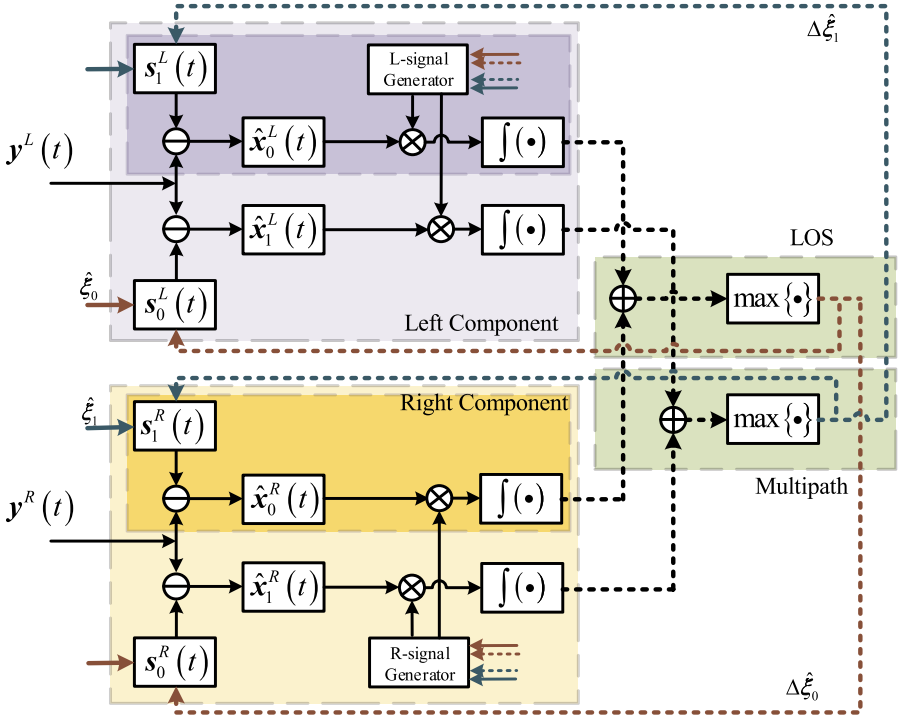

Fig. 7. The proposed SAGE-based discriminator for meta-signal.

$$\hat{R}^L_{\theta,0}\left(\Delta\theta^L_0\right)=\frac{1}{T}\int_0^T\left(\boldsymbol{a}^L\left(\hat{\theta}_0+\Delta\theta^L_0\right)\right)^H\hat{\boldsymbol{x}}^L_0(t)\times\left(c^L\left(t-\hat{\tau}_0\right)e^{-j2\pi f_s\left(t-\hat{\tau}_0\right)}e^{j\left(2\pi\hat{f}_{d,0}t+\hat{\phi}_0\right)}\right)^H dt \tag{9a}$$

$$\hat{R}^L_{\tau,0}\left(\Delta\tau^L_0\right)=\frac{1}{T}\int_0^T\left(\boldsymbol{a}^L\left(\hat{\theta}_0\right)\right)^H\hat{\boldsymbol{x}}^L_0(t)\times\left(c^L\left(t-\hat{\tau}_0+\Delta\tau^L_0\right)e^{-j2\pi f_s\left(t-\left(\hat{\tau}_0+\Delta\tau^L_0\right)\right)}e^{j\left(2\pi\hat{f}_{d,0}t+\hat{\phi}_0\right)}\right)^H dt \tag{9b}$$

$$\hat{P}^L_{\phi,0}\left(\Delta\phi^L_0\right)=\frac{1}{T}\int_0^T\left(\boldsymbol{a}^L\left(\hat{\theta}_0\right)\right)^H\hat{\boldsymbol{x}}^L_0(t)\times\left(c^L\left(t-\hat{\tau}_0\right)e^{-j2\pi f_s\left(t-\hat{\tau}_0\right)}e^{j\left(2\pi\hat{f}_{d,0}t+\left(\hat{\phi}_0+\Delta\phi^L_0\right)\right)}\right)^H dt \tag{9c}$$

$$\Delta\hat{\alpha}^L_0=\left|\frac{1}{T}\int_0^T\left(\boldsymbol{a}^L\left(\hat{\theta}_0\right)\right)^H\hat{\boldsymbol{x}}^L_0(t)\times\left(c^L\left(t-\hat{\tau}_0\right)e^{-j2\pi f_s\left(t-\hat{\tau}_0\right)}e^{j\left(2\pi\hat{f}_{d,0}t+\hat{\phi}_0\right)}\right)^H dt\right|\Big/M_\theta \tag{9d}$$

where the Doppler frequency $\hat{f}_{d,0}$ and carrier phase offsets $\hat{\phi}_0$ for the LOS ray of the meta-signal are acquired by standard PLLs, and $\Delta\hat{\phi}_0$ for the LOS ray of the left side-band component is estimated by the left side-band prompt correlator. It is worth noting that no significant DFO difference (generally within a few Hertz) was found between the LOS ray and multipath rays, as verified in several practical measurements [45–47]. Without loss of generality, we can reasonably assume that the LOS ray and the multipath rays have similar DFOs, and most of the DFOs will be compensated in the acquisition stage [48]. Starting with the fundamental fact that the residual DFOs are very similar for all rays, we cannot profit much from the frequency offsets for multipath mitigation. To reduce the complexity, the rays are mainly resolved from the spatial and temporal ACF correlators. Meanwhile, we set up PLLs to complete the carrier tracking as well. Thanks to these PLLs, the architecture of SAGELL incorporates frequency discrimination of the rays if the frequency separation of the rays is larger than the bandwidth of PLLs.

Similarly, the expressions for the multipath signal of left component $\left\{\hat{R}^L_{\theta,1}\left(\Delta\theta^L_1\right),\hat{R}^L_{\tau,1}\left(\Delta\tau^L_1\right),\hat{P}^L_{\phi,1}\left(\Delta\phi^L_1\right),\Delta\hat{\alpha}^L_1\right\}$, the LOS ray $\left\{\hat{R}^R_{\theta,0}\left(\Delta\theta^R_0\right),\hat{R}^R_{\tau,0}\left(\Delta\tau^R_0\right),\hat{P}^R_{\phi,0}\left(\Delta\phi^R_0\right),\Delta\hat{\alpha}^R_0\right\}$, and $\left\{\hat{R}^R_{\theta,1}\left(\Delta\theta^R_1\right),\hat{R}^R_{\tau,1}\left(\Delta\tau^R_1\right),\hat{P}^R_{\phi,1}\left(\Delta\phi^R_1\right),\Delta\hat{\alpha}^R_1\right\}$ for the multipath ray of right component of the meta-signal will not be displayed anymore. Moreover, the amplitudes $\Delta\hat{\alpha}^L_k$ and $\Delta\hat{\alpha}^R_k$ for each ray each side-band component are kept to the next iteration.

4.2.2. Meta-signal processing unit

To improve accuracy, a coherent combination according to the ACF of the meta-signal (2), including the spatial ACFs $\left\{\hat{R}^L_{\theta,k}\left(\Delta\theta^L_k\right),\hat{R}^R_{\theta,k}\left(\Delta\theta^R_k\right)\right\}$, the temporal ACFs $\left\{\hat{R}^L_{\tau,k}\left(\Delta\tau^L_k\right),\hat{R}^R_{\tau,k}\left(\Delta\tau^R_k\right)\right\}$, is conducted to acquire the angles $\Delta\hat{\theta}_k$ and time delays $\Delta\hat{\tau}_k$ estimates of the meta-signal,

$$\Delta\hat{\theta}_k=\arg\max_{\Delta\theta}\left|\gamma\hat{R}^L_{\theta,k}\left(\Delta\theta^L_k\right)+\hat{R}^R_{\theta,k}\left(\Delta\theta^R_k\right)\right| \tag{10}$$

$$\Delta\hat{\tau}_k=\arg\max_{\Delta\tau}\left|\gamma\hat{R}^L_{\tau,k}\left(\Delta\tau^L_k\right)+\hat{R}^R_{\tau,k}\left(\Delta\tau^R_k\right)\right| \tag{11}$$

with the compensation γ for unequal powers of two components, which is necessary to know the amplitude ratio between two sig-

nals [33]. This coherent combination for the LOS ray and the multipath ray of the meta-signal is mentioned in Fig. 7 as well.

Moreover, the prompt correlators $\left\{\hat{P}^{L}_{\phi,k}\left(\Delta\phi^{L}_{k}\right), \hat{P}^{R}_{\phi,k}\left(\Delta\phi^{R}_{k}\right)\right\}$ for each ray of each component are sent to incoherently estimate the carrier phases of the meta-signals,

$$\Delta\hat{\phi}_{k} = \frac{1}{2}\left(\text{angle}\left(\hat{P}^{L}_{\phi,k}\left(\Delta\phi^{L}_{k}\right)\right) + \text{angle}\left(\hat{P}^{R}_{\phi,k}\left(\Delta\phi^{R}_{k}\right)\right)\right) \tag{12}$$

The meta-signal parameters obtained above, the amplitudes for each ray of each component, together with the prediction results tracked through the last loop, are sent back to the SAGE-based discriminator for initialization. Inside the SAGE-based discriminator, the first two kinds of variables are updated until the convergence criteria get satisfied. Afterwards, they are filtered and predicted through various loops to get more accurate estimates and fed back to initialize the SAGE-based discriminator eventually.

5. Simulation results

In this section, we provide two kinds of simulation experiments to evaluate the performance of three methods. Firstly, the MEE experiments are arranged to indicate the ultimate time delay bias. Secondly, the simulations of time delay RMSE via C/N_0 in different multipath cases are shown. The typical combination of Beidou B1I and B1C signals is considered for the targeted meta-signal. The subcarrier frequency offset f_s locates at 7.161 MHz.

Three DSB methods are adopted in the simulation experiments: the MEDLL [7], the Double Estimator Technique (DET) based technique [32], [33] and the proposed SAGELL. In the MEDLL for meta-signal, we first iteratively acquire the temporal ACF and the prompt correlator for the LOS ray and the multipath ray of each sideband component according to the equations (9b) and (9c), then coherently and incoherently combine the time delay estimates and carrier phases according to the equations (11) and (12), respectively. Finally, the DLLs with Early-Late discriminator and PLLs are utilized to track each ray of the meta-signal. A four-element uniform linear array (ULA) with a half-wavelength antenna spacing is assumed. To make a relatively fair comparison, we make beamforming to the LOS direction before conducting the conventional MEDLL and DET, and the detailed ACF distortion before and after beamforming are described in reference [11]. Generally, the multipath distortion after beamforming can be further relieved by the temporal multipath-mitigating methods.

Under the assumption of two rays (one LOS ray and one multipath ray), we suppose four multipath scenarios that are differentiated by the angles and the time delays. For angles, we consider two cases: one is with large angle difference that the angle of LOS ray is from 0° and the multipath ray is from 40°, and the other one is with small angle difference that the angle of LOS ray is from 0° and the multipath ray is from 10°. Likewise, we consider two cases in time delays: one is with large delay difference that the time delay of LOS ray is $0T_c$ and the multipath ray is $0.08T_c$, and the other one is with small delay difference that the time delay of LOS ray is $0T_c$ and the multipath ray is $0.007T_c$. The denotation T_c refers to the time duration $T_c = 977.52$ ns of two adjacent chips per C/A code period.

The signal-to-multipath ratio is set to be 6 dB.[2] The pre-detection integration time T is 20 milliseconds. The noise bandwidth parameters of angle, delay, and carrier tracking lock loops are 5 Hz, 5 Hz, and 10 Hz, respectively. All the lock loops' order are second order. The early-late spacing in the DLL of DET are

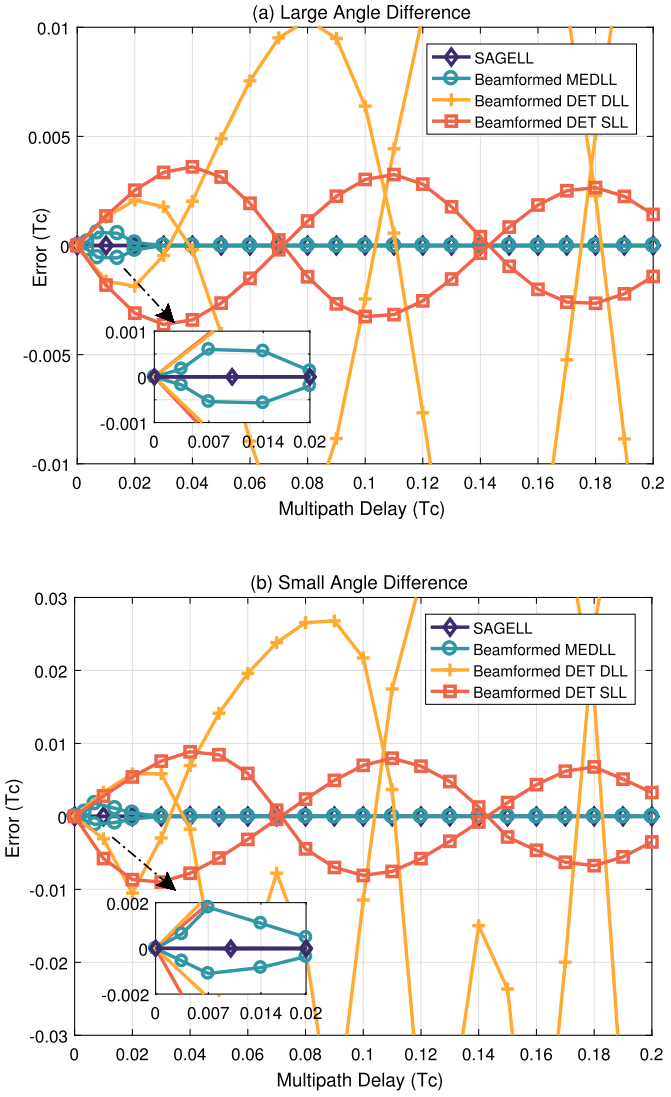

Fig. 8. MEEs of LOS ray with large angle difference (a) or small angle difference (b).

$0.5T_c$ and $0.33T_c$ for B1I and B1C signals, respectively. And that of MEDLL is set to be $0.034T_c$.

5.1. Case A: MEEs via multipath delay

In this subsection, the MEEs of the LOS ray with large angle difference and small angle difference between the LOS ray and multipath ray are demonstrated.

It is apparent from Fig. 8 that the MEEs with large angle difference generally behave about twice as large as that with small angle difference. Among these three comparisons, the beamformed DET reveals a comparatively poor multipath mitigation with small angle difference and large one. A possible explanation is that the beamforming cannot thoroughly mitigate the multipath ray. Thus, the residual multipath still causes quite a considerable influence on subcarrier phase tracking of the LOS ray. The error of beamformed MEDLL, by contrast, maintains a competitive advantage out of the range $[0T_c, 0.02T_c]$ irrespective of the similarity in spatial domain. However, the curves of the beamformed MEDLL in the range $[0T_c, 0.02T_c]$ rise and fall drastically, and they peak at nearly $0.007T_c$ reaching $0.6m$. By only time domain characteristics, the method MEDLL cannot eliminate the multipath under the condition of two highly temporally correlated rays. Besides, beamforming contributes to multipath mitigation when the low spatially

[2] A relatively strong multipath amplitude is used to make the effects of the multipath signals and the proposed methods more evident.

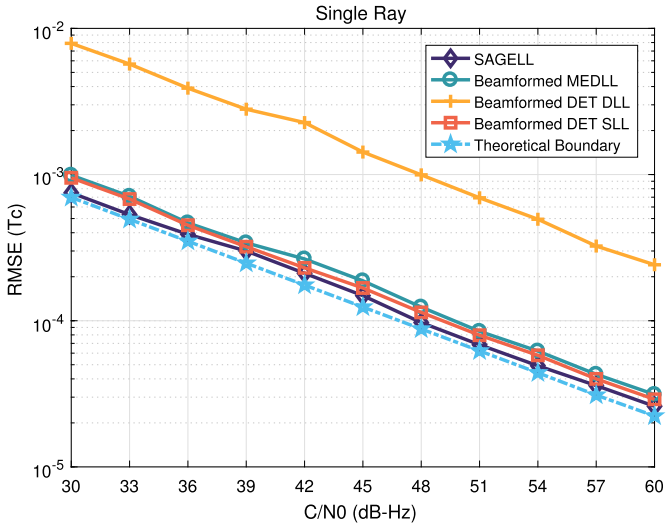

Fig. 9. Delay RMSEs comparison of single ray.

correlated rays exist, but it offers a poor attenuation a highly spatially correlated situation. A direct consequence of combining multiple dimensions is that SAGELL observes and differentiates the multipath from both spatial and temporal domains, so it exhibits reasonably good performance.

5.2. Case B: RMSE via C/N_0

In order to evaluate and compare the thermal noise performance, five specific simulated scenarios are set, and the RMSEs of the LOS ray are exploited in this section. These five scenarios conclude single ray, large angle difference within small delay difference and large delay difference, together with small angle difference within small delay difference and large delay difference. The other settings are the same as those in the previous section.

In Fig. 9, the comparisons of the LOS time delay RMSEs among three methods in single ray (i.e., LOS only) scenario and the theoretical boundary of the meta-signal are shown. Since the single ray is set, the beamforming in this scenario plays a crucial role in the signal gain increase instead of multipath mitigation. The theoretical boundary with a single-antenna can be plotted according to [49], and the theoretical boundary with a four-element antenna could be derived easily. The curves show that these methods yielded the best values, especially the SAGELL and the SLL of DET, almost reaching the theoretical boundary. Given the fact that SAGELL adopts an iterative multiple correlators discriminator in multi-dimensions, whereas the DET and MEDLL use prompt or Early-Late discriminators in temporal domain, the complexity of SAGELL slightly exceeds that of the MEDLL.

Next, the RMSEs of the LOS time delay in four multipath scenarios are presented. The trend of beamformed MEDLL corresponds to the fact that it can differentiate the multipath in large time delay difference in the previous analysis of MEE, which are shown in the left-hand side plots in Fig. 10(a) and Fig. 11(a). However, this fact is in contrast with the behaviors of the beamformed MEDLL in a small delay difference scenario. The beamformed MEDLL suffers from limitations of only resolving multipath via time delays, especially in the presence of highly spatially and temporally correlated rays, as displayed by the right panel in Fig. 11(b).

Unlike other methods carried out in this case, SAGELL is found to perform exceptionally well with high C/N_0, benefiting from spatial, and temporal domains. Despite the appearance of the meta-signal ambiguity in the low C/N_0 range [26], the SAGELL has basically reached a centimeter-level ranging performance at 39 dB-Hz.

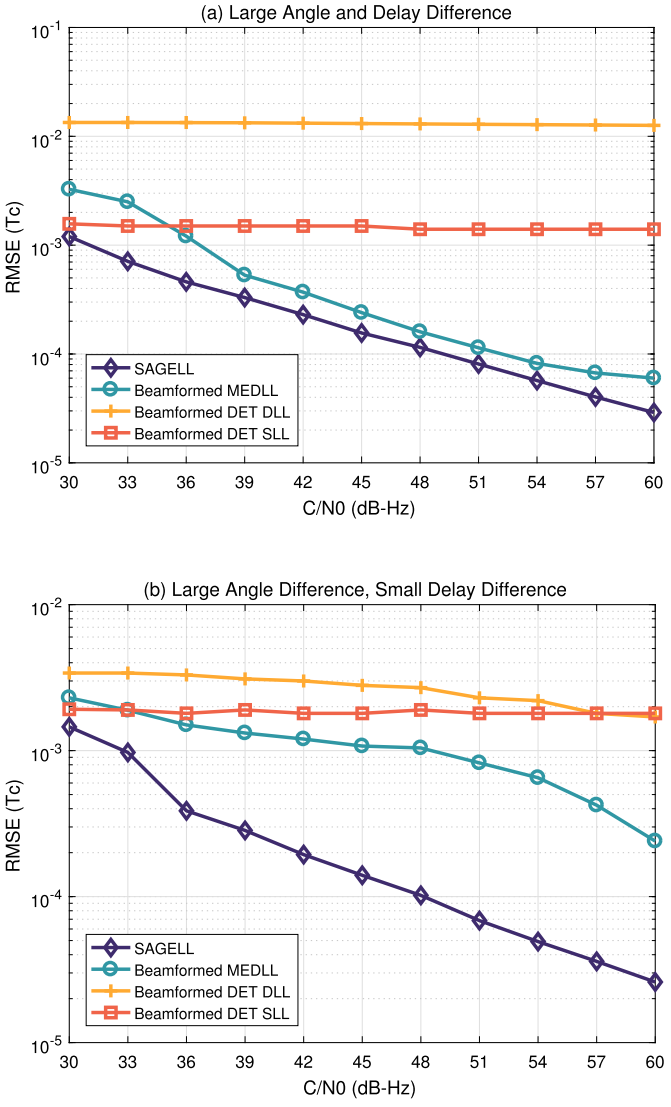

Fig. 10. Delay RMSEs of LOS signal comparison when LOS and multipath are separate from 0° and 40°, respectively, with large delay difference $0.08T_c$ (a) and small delay difference $0.007T_c$ (b).

6. Conclusion

The problem of time delay estimation in the presence of severe multipath propagation has been analyzed, showing that optimum time delay can be found by combining multi-dimensional processing and wide bandwidth. Therefore, we propose the SAGELL design inspired by the robustness of SAGE against multipath and excellent temporal resolution of the meta-signal. With the basic principles of SAGE, the SAGE-based discriminator iteratively combats the multipath from joint spatial and temporal domains and forms the precise estimates of the meta-signal coherently. To maintain the high accuracy in multipath mitigation, a variety of loops: the ALLs, DLLs, and PLLs, are fitting to track and predict the rays for SAGELL. Simulation results show that the proposed SAGELL reaches the theoretical bound in only one LOS ray propagating environment and performs a remarkable multipath mitigation capacity, especially in the presence of both small time delay difference and angle difference of the LOS ray and the multipath ray.

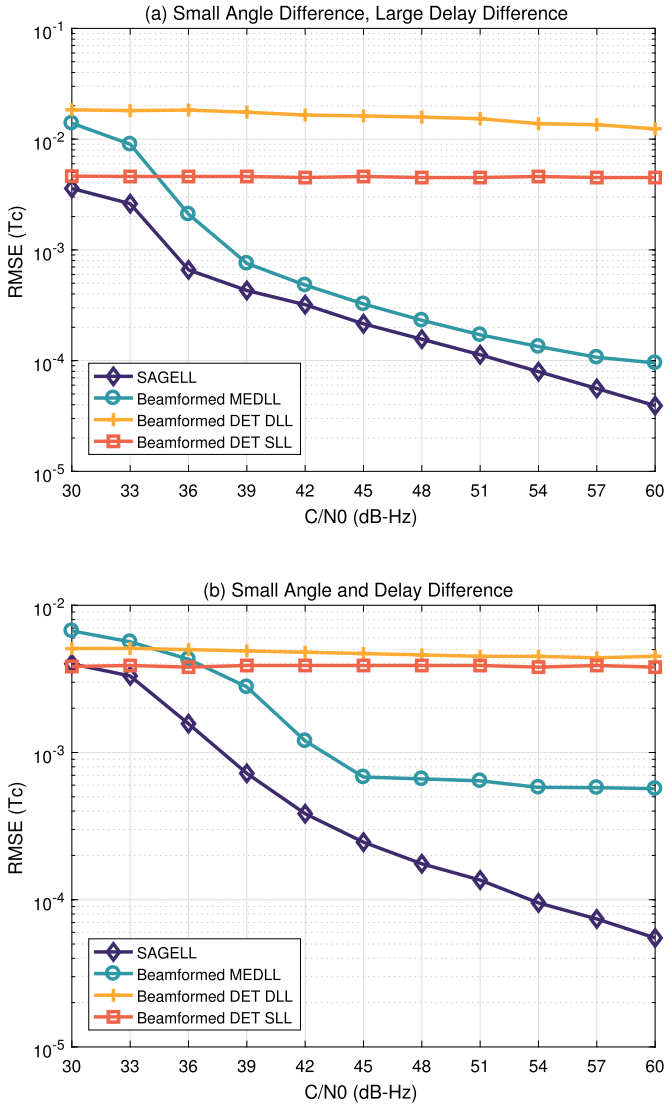

Fig. 11. Delay RMSEs of LOS signal comparison when LOS and multipath are similar from 0° and 10°, respectively, with large delay difference $0.08T_c$ (a) and small delay difference $0.007T_c$ (b).

CRediT authorship contribution statement

Ning Chang: Conceptualization, Methodology, Software, Writing. **Xi Hong**: Software, Validation, Formal Analysis. **Wenjie Wang**: Validation, Supervision. **Gonzalo Seco-Granados**: Methodology, Review & Editing, Supervision.

Declaration of competing interest

The authors declare that they have no known competing financial interests or personal relationships that could have appeared to influence the work reported in this paper.

Data availability

No data was used for the research described in the article.

Acknowledgment

This study is funded in part by the Spanish Ministry of Science and Innovation Projects under Grant PID2020-118984GB-I00, and in part by the Catalan Catalan ICREA Academia Programme under Grant IC-Academia 2019.

References

[1] R.D.J. van Nee, Multipath effects on GPS code phase measurements, Navigation 39 (2) (1992) 177–190.
[2] S. Kalyanaraman, M. Braasch, J. Kelly, Code tracking architecture influence on GPS carrier multipath, IEEE Trans. Aerosp. Electron. Syst. 42 (2) (2006) 548–561.
[3] R. Wu, W. Wang, D. Lu, L. Wang, Q. Jia, Adaptive Interference Mitigation in GNSS, Springer, Singapore, 2018.
[4] T. Kos, I. Markezic, J. Pokrajcic, Effects of multipath reception on GPS positioning performance, in: Proceedings ELMAR-2010, 2010, pp. 399–402.
[5] K. Larson, D. Akos, L. Marti, Characterizing multipath from satellite navigation measurements in urban environments, in: 2008 5th IEEE Consumer Communications and Networking Conference, 2008, pp. 620–625.
[6] A.J.V. Dierendonck, P. Fenton, T. Ford, Theory and performance of narrow correlator spacing in a GPS receiver, Navigation 39 (3) (1992) 265–283.
[7] R. van Nee, The multipath estimating delay lock loop, in: IEEE Second International Symposium on Spread Spectrum Techniques and Applications, IEEE, 1994.
[8] B.R. Townsend, P.C. Fenton, K.J.V. Dierendonck, D.J.R. van Nee, Performance evaluation of the multipath estimating delay lock loop, Navigation 42 (3) (1995) 502–514.
[9] T. Kailath, ESPRIT–estimation of signal parameters via rotational invariance techniques, Opt. Eng. 29 (4) (1990) 296.
[10] N. Chang, X. Hong, W. Wang, Z. Wang, Subspace based joint delay and direction of arrival estimation for GNSS multipath signals, in: China Satellite Navigation Conference (CSNC) 2018 Proceedings, 2018.
[11] X. Hong, W. Wang, N. Chang, Q. Yin, A subspace-based code tracking loop design for GPS multi-antenna receiver in multipath environment, GPS Solut. 24 (4) (aug 2020).
[12] Z. Zhang, B.D. Rao, Sparse signal recovery with temporally correlated source vectors using sparse Bayesian learning, IEEE J. Sel. Top. Signal Process. 5 (5) (2011) 912–926.
[13] N. Chang, W. Wang, X. Hong, J.A. López-Salcedo, G. Seco-Granados, Joint angle and delay estimation for GNSS multipath signals based on multiple sparse Bayesian learning, GPS Solut. 25 (2) (feb 2021).
[14] S. Pillai, B. Kwon, Forward/backward spatial smoothing techniques for coherent signal identification, IEEE Trans. Acoust. Speech Signal Process. 37 (1) (1989) 8–15.
[15] S. Fortunati, R. Grasso, F. Gini, M.S. Greco, K. LePage, Single-snapshot DOA estimation by using compressed sensing, EURASIP J. Adv. Signal Process. 2014 (1) (2014) 120.
[16] G. Seco Granados, Antenna Arrays for Multipath and Interference Mitigation in GNSS Receivers, Universitat Politècnica de Catalunya, 2000.
[17] G. Seco-Granados, J. Fernandez-Rubio, C. Fernandez-Prades, ML estimator and hybrid beamformer for multipath and interference mitigation in GNSS receivers, IEEE Trans. Signal Process. 53 (3) (2005) 1194–1208.
[18] F. Antreich, J. Nossek, W. Utschick, Maximum likelihood delay estimation in a navigation receiver for aeronautical applications, Aerosp. Sci. Technol. 12 (3) (2008) 256–267.
[19] B. Fleury, M. Tschudin, R. Heddergott, D. Dahlhaus, K.I. Pedersen, Channel parameter estimation in mobile radio environments using the SAGE algorithm, IEEE J. Sel. Areas Commun. 17 (3) (1999) 434–450.
[20] F. Antreich, J.A. Nossek, G. Seco-Granados, A.L. Swindlehurst, The extended invariance principle for signal parameter estimation in an unknown spatial field, IEEE Trans. Signal Process. 59 (7) (2011) 3213–3225.
[21] J.-L. Issler, M. Paonni, B. Eissfeller, Toward centimetric positioning thanks to L- and S-band GNSS and to meta-GNSS signals, in: 2010 5th ESA Workshop on Satellite Navigation Technologies and European Workshop on GNSS Signals and Signal Processing (NAVITEC), IEEE, 2010.
[22] M. Paonni, J. Curran, M. Bavaro, J. Fortuny-Guasch, GNSS meta signals: coherently composite processing of multiple GNSS signals, in: Proceedings of the 27th International Technical Meeting of the Satellite Division of the Institute of Navigation (ION GNSS+ 2014), 2014, pp. 2592–2601.
[23] J. Garcia-Molina, M. Navarro-Gallardo, G. Lopez-Risueño, M. Crisci, Unambiguous tracking of high-order BOC signals in urban environments: channel considerations, in: 2014 7th ESA Workshop on Satellite Navigation Technologies and European Workshop on GNSS Signals and Signal Processing (NAVITEC), IEEE, 2014, pp. 1–6.
[24] Z. Liu, B. Li, X. Zhu, L. Li, G. Sun, Band-pass sampling in high-order BOC signal acquisition, Appl. Sci. 8 (11) (2018) 2226.
[25] R. Weiler, P. Blunt, M. Unwin, S. Hodgart, A direct-conversion receiver for wideband GNSS signals, in: GNSS Signals & Signal Processing Workshop, Toulouse, France, 2008.
[26] P. Das, L. Ortega, J. Vilà-Valls, F. Vincent, E. Chaumette, L. Davain, Performance limits of GNSS code-based precise positioning: GPS, Galileo & meta-signals, Sensors 20 (8) (2020) 2196.

[27] L. Ortega, D. Medina, J. Vilà-Valls, F. Vincent, E. Chaumette, Positioning performance limits of GNSS meta-signals and HO-BOC signals, Sensors 20 (12) (2020) 3586.
[28] D.M. Akos, A. Ene, J. Thor, A prototyping platform for multi-frequency GNSS receivers, in: Proceedings of the 16th International Technical Meeting of the Satellite Division of the Institute of Navigation (ION GPS/GNSS 2003), 2003, pp. 117–128.
[29] M.S. Hodgart, P.D. Blunt, M. Unwin, Double estimator—a new receiver principle for tracking BOC signals, Inside GNSS 3 (3) (2008) 26–36.
[30] W. Li, Y. Wang, R. Chen, M. Liu, Anti-multipath dual-estimate loop method for boc modulated signals, Syst. Eng. Electron. (2018).
[31] Y. Zhu, X. Cui, M. Lu, Dual binary phase-shift keying tracking method for Galileo E5 AltBOC(15, 10) signal and its thermal noise performance, IET Radar (2015).
[32] D. Borio, Double phase estimator: new unambiguous binary offset carrier tracking algorithm, IET Radar Sonar Navig. 8 (7) (2014) 729–741.
[33] C. Wang, X. Cui, T. Ma, S. Zhao, M. Lu, Asymmetric dual-band tracking technique for optimal joint processing of BDS B1I and B1C signals, Sensors 17 (10) (2017) 2360.
[34] Y. Gao, Z. Yao, M. Lu, High-precision unambiguous tracking technique for BDS B1 wideband composite signal, Navigation 67 (3) (2020) 633–650.
[35] J.W. Betz, Binary offset carrier modulation for radionavigation, Navig., J. Inst. Navig. 48 (4) (2001) 227–246.
[36] H. Akaike, A new look at the statistical model identification, IEEE Trans. Autom. Control 19 (6) (1974) 716–723.
[37] M. Wax, T. Kailath, Detection of signals by information theoretic criteria, IEEE Trans. Acoust. Speech Signal Process. (1985).
[38] S. Kritchman, B. Nadler, Non-parametric detection of the number of signals: hypothesis testing and random matrix theory, IEEE Trans. Signal Process. 57 (10) (2009) 3930–3941.
[39] M. Zhang, S. Zhu, X. Chen, A. Zhang, Fast detection of the number of signals based on Ritz values: a noise-power-aided approach, IEEE Trans. Aerosp. Electron. Syst. 58 (1) (2022) 651–662.
[40] G.X. Gao, S. Datta-Barua, T. Walter, P. Enge, Ionosphere effects for wideband GNSS signals, in: Proceedings of the 63rd Annual Meeting of the Institute of Navigation (2007), 2007, pp. 147–155.
[41] U. Hörmann, S. Thoelert, M. Sgammini, C. Enneking, J. Furthner, M. Meurer, F. Antreich, Ionospheric deformation of broadband GNSS signals and its analysis with a high gain antenna, GPS Solut. 22 (4) (2018) 1–11.
[42] N. Guo, Y. Kou, Y. Zhao, Z. Yu, Y. Chen, An all-pass filter for compensation of ionospheric dispersion effects on wideband GNSS signals, GPS Solut. 18 (4) (2014) 625–637.
[43] L. Du, T. Yardibi, J. Li, P. Stoica, Review of user parameter-free robust adaptive beamforming algorithms, Digit. Signal Process. 19 (4) (2009) 567–582.
[44] E.D. Kaplan, C.J. Hegarty, Understanding GPS: Principles and Applications, 3rd edn, Artech House, 2017.
[45] M. Irsigler, Characterization of multipath phase rates in different multipath environments, GPS Solut. 14 (4) (2010) 305–317.
[46] H. Keshvadi, A. Broumandan, G. Lachapelle, Spatial characterization of GNSS multipath channels, Int. J. Antennas Propag. 2012 (2012) 1–15.
[47] P. Xie, M.G. Petovello, Measuring GNSS multipath distributions in urban canyon environments, IEEE Trans. Instrum. Meas. 64 (2) (2015) 366–377.
[48] A.J. O'Brien, Adaptive antenna arrays for precision GNSS receivers, Ph.D. thesis, The Ohio State University, 2010.
[49] J.W. Betz, K.R. Kolodziejski, Generalized theory of code tracking with an early-late discriminator part I: lower bound and coherent processing, IEEE Trans. Aerosp. Electron. Syst. 45 (4) (2009) 1538–1556.

Ning Chang received B.S. and M.S. in communication engineering from Information Engineering University, China, 2011 and Xidian University, China, 2014, respectively. She is currently pursuing the double Ph.D. degree in Information and Communication Engineering at Xi'an Jiaotong University and in Electronic and Telecommunication Engineering at Universitat Autònoma de Barcelona. Her research interests include compressed sensing, array signal processing, parameter estimation and multipath mitigation for GNSS signals.

Xi Hong received a B.S. and Ph.D. degrees from the School of Electronics and Information Engineering, Xi'an Jiaotong University, Xi'an, China, in 2012 and 2022, respectively. He has been a faculty member with Xi'an Jiaotong University since 2022. His main research interests include array signal processing, signal processing in communication systems, multipath mitigation in navigation, and GNSS physical layer interference detection.

Wenjie Wang received the B.S., M.S., and Ph.D. degrees in information and communication engineering from Xi'an Jiaotong University, Xi'an, China, in 1993, 1998, and 2001, respectively, where he is currently a Professor. His main research interests include information theory, broadband wireless communications, signal processing in communication systems, and array signal processing.

Gonzalo Seco-Granados received the Ph.D. degree in telecommunications engineering from the Universitat Politecnica de Catalunya, Spain, in 2000, and the M.B.A. degree from the IESE Business School, Spain, in 2002. He is currently a Professor with the Department of Telecommunication, Universitat Autonoma de Barcelona, where he served as the Vice Dean of the Engineering School, from 2011 to 2019. His research interests include statistical and array signal processing for GNSS and 5G-based localization systems, multipath and spoofing mitigation, and low-energy positioning. Since 2019, he has been the President of the Spanish Chapter of the IEEE Aerospace and Electronic Systems Society. He received the ICREA Academia award in 2013 and 2019.